A One-Dimensional Heat, Mass and Charge Transfer Model for a Polymer Electrolyte Fuel Cell Stack

Colleen Spiegel

Abstract

A one-dimensional heat, mass and charge transfer model was developed for a polymer electrolyte fuel cell stack to predict the temperatures, mass flows, pressure drops, and charge transport of each fuel cell layer over different operating conditions. The fuel cell layers' boundaries were connected to form the overall stack model.

The numerical model was validated using a 16 cm^2 active area single cell fuel cell stack. The properties of each stack layer, the gases and the surroundings were input into the numerical model. Results showed that the numerical prediction for temperatures of the fuel cell layers, and the overall polarization curve agrees well (average error of 1%) with the fuel cell layer temperatures measured.

Keywords: Mathematical model; PEM fuel cell; PEFC; Stack; Thermal model

1.0 Introduction

There are many areas of fuel cell technology that need to be improved for it to become commercially viable. Some of these areas include fuel cell water management, heat generation, adequate mass transport to the electrodes and optimization of charge transport through the fuel cell layers – which all affect the overall fuel cell performance. All these fuel cell parameters are interdependent, and vary with operating conditions, stack design

and balance of plant. Variance in fuel cell stack temperatures are a result of water phase change, coolant temperature, air convection, the trapping of water, and heat produced by the catalyst layer. The membrane must be adequately hydrated for proper ionic conduction through the fuel cell. If the fuel cell is heated too much, the water in the fuel cell will evaporate, the membrane will dry out, and the performance of the fuel cell will suffer. If too much water is produced on the cathode side, water removal can become a problem, and this affects the overall cell heat distribution. This ultimately leads to fuel cell performance losses. To precisely predict the overall fuel cell performance, the temperatures, concentrations of the species and rates of reaction, the energy, mass and charge throughout the stack needs to be determined accurately.

Mass transfer through the different fuel cell layers can greatly affect fuel cell performance. The fuel cell must be supplied continuously with fuel and oxidant, and product water must be removed continually to insure proper fuel and oxidant at the catalyst layers to maintain high fuel cell efficiency. High fuel and oxidant flow rates sometimes insure good distribution of reactants, but if the flow rate is too high, the fuel may move too fast to diffuse through the GDL and catalyst layers. If it is too low, the fuel cell will lose efficiency. Mass transport in the fuel cell GDL and catalyst layers are dominated by diffusion due to the tiny pore sizes of these layers (2 to 10 microns). In a flow channel, the velocity of the reactants is usually slower near the walls; therefore, this aids the flow change from convective to diffusive.

The transport of charges is also very important since efficient charge transport ensures the highest possible electricity produced by the fuel cell stack. The two major types of

charged particles are electrons and ions, and both electronic and ionic losses occur in the fuel cell. The electronic loss between the bipolar, cooling and contact plates are due to the degree of contact that the plates make with each other due to the compression of the fuel cell stack. The ionic losses occur in the membrane, therefore, ensuring optimal ionic transport is critical for good fuel cell performance. To optimize the mass, heat and charge transport to obtain the best electrochemical performance, detailed experimentation and modeling are needed.

The objective of this paper is to develop a one-dimensional numerical model for predicting the heat, mass and charge transport through the layers of the fuel cell stack. The results of the numerical model will be experimentally validated to study the combined effect of these parameters on the performance of a PEM fuel cell. The numerical model consists of the calculation of the both conductive and convective transient heat transfer, transient mass transfer, charge transfer, pressure drop, a porous catalyst model and an empirical membrane model based upon the model developed by Springer et al. Both the thermal part of the model, and the overall electrochemical model were validated in this study. The experimental validation of the thermal model consists of heating of an aluminum heating next to the anode end plate to a certain temperature, and then letting it cool through natural convection over time. The experimental validation for the overall model consists of obtaining I-V curves under varying temperatures. The motivation of this work was to build a transient model that can be used to examine the effects of thermal diffusion, catalyst heating, membrane hydration, species and charge transport and material design, selection and optimization for a fuel cell stack.

2.0 Model development

A single cell fuel cell stack consists of two end plates, contact and gasket layers, two flow field plates, two layers of diffusion media, two catalyst layers and a membrane layer. The schematic of a typical PEFC stack is shown in Fig. 1 [10].

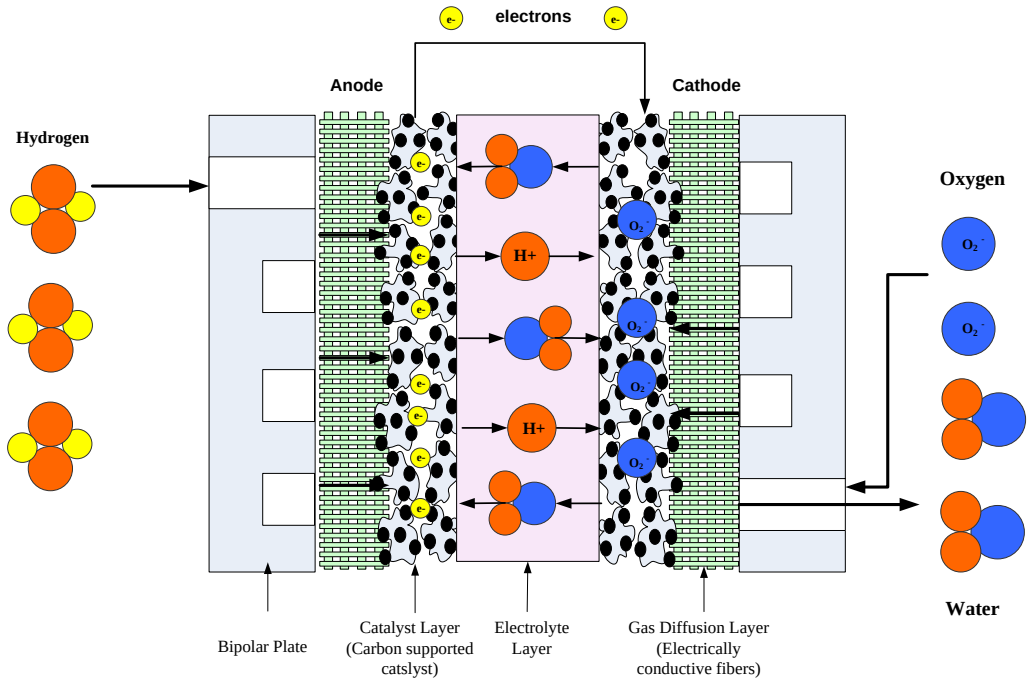

Fig. 1. Schematic of a Polymer Electrolyte Membrane Fuel Cell (PEMFC) Stack

2.1. Model assumptions

The following assumptions were made for the numerical model:

1. The heat, mass and charge transfer in the stack is one-dimensional (x-direction).

2. All material thermal properties are constant over the temperature range considered (20 to 80 °C).

3. The air and hydrogen flow are assumed to come directly into the flow field plates.

4. For the MEA layers, only the active area was included in the model. The materials surrounding the MEA were not included in the model.

2.2. Numerical model approach

An illustration of the fuel cell stack, and the control volume approach is shown in Fig. 2 and Fig. 3. Each control volume is assumed to abut the next one in the x-direction [10]. The stack model is coded to enable the user to input the desired number of control volumes per layer.

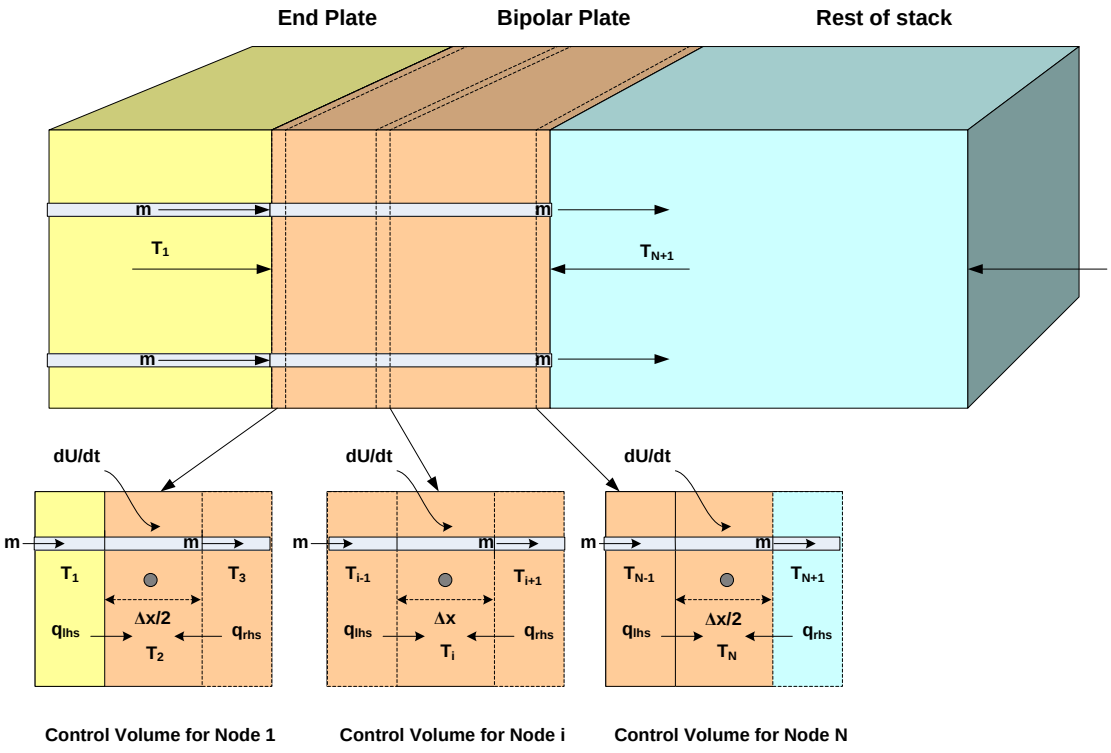

Fig. 2. Schematic of the PEFC stack and its components for one-dimensional model development.

The model obtains the temperatures at the center of each control volume, and the mass flow rates, pressure drop, velocity and charge transport at the boundaries of each control volume as shown in Fig. 2. The detailed governing equations for each layer are discussed in the remainder of this paper.

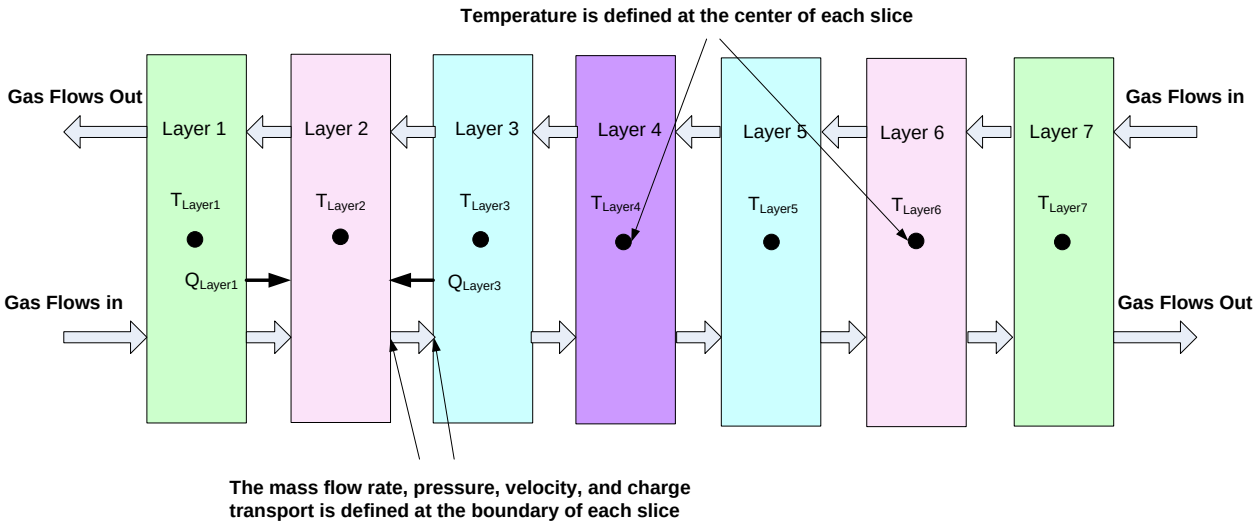

Fig. 3. Illustration of the modeling boundaries for numerical model

2.2. Equations for each layer

2.2.1. End plates, contacts and gasket materials

The end plate provides support to the fuel cell layers, and uniformly transmits the compressive forces to the fuel cell stack. It is typically made of a metal or polymer material. The fuel cell stack also typically has contact and gasket layers, which vary in design and material. The gasket layers help to prevent gas leaks and improve stack compression. The contact layers or current collectors are used to collect electrons from the bipolar plate and gas diffusion layer (GDL) [10].

Depending upon the stack design, there could be gas or liquid flows in the end plates, gaskets or contact layers. Including the effect of pressure drop and the change in velocity of the flows through these layers are minimal and are typically neglected in model. However, the temperature of these layers can affect the temperature of the internal layers (or vice versa), therefore, they will be included in this model.

One side of each of these layers is exposed to an insulating material (or the ambient environment), and the other side is exposed to a conductive current collector plate or insulating material. Conduction is the main mode of heat transfer in the layer materials. However, there will also be a small amount of convective heat transfer if there is a flow channel in a layer. A charge balance only needs to be conducted on the layer if it will conduct electrons. An illustration of the mass, energy and charge balances on a layer are shown in Fig. 4 [10].

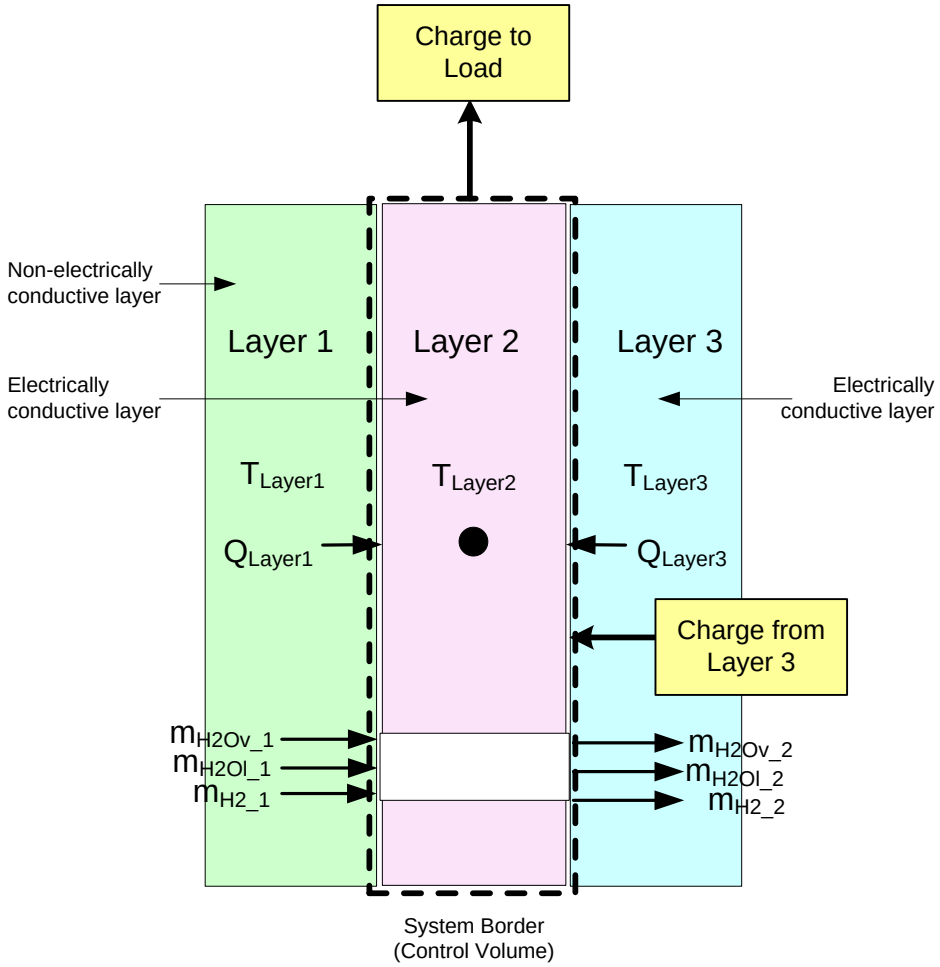

Fig. 4. Mass, energy and charge balance around a layer

The general energy balance for the end plate, contact and GDL layers can be written as:

$$(\rho_{Layer\,2} A_{Layer\,2} t_{Layer\,2} cp_{Layer\,2}) \frac{dT_{Layer\,2}}{dt} = Q_{Layer\,1} + Q_{Layer\,3} \tag{1}$$

where $\rho_{Layer\,2}$ is the density of Layer2, $A_{Layer\,2}$ is the area of Layer2, $cp_{Layer\,2}$ is the specific heat capacity of Layer2, $Q_{Layer\,1}$ is the heat flow from Layer1 and $Q_{Layer\,3}$ is the heat flow from Layer3. The derivative on the left side is the rate of change of control volume temperature ($dT_{Layer\,2} / dt$). The heat flow from Layer1 to Layer 2 is [10, 11]:

$$Q_{Layer\,1} = U_{Layer\,1} A(T_{Layer\,1} - T_{Layer\,2}) \tag{2}$$

where $U_{Layer\,1}$ is the overall heat transfer coefficient for Layer1, A is the area of the layer and T is the temperature of the layer. The heat flow from Layer3 to Layer 2 can be expressed as:

$$Q_{Layer\,3} = U_{Layer\,3} A(T_{Layer\,3} - T_{Layer\,2}) \tag{3}$$

If the heat is coming from the surroundings, the overall heat transfer coefficient can be calculated by:

$$U_{surr} = \frac{1}{\frac{t_{Layer\,2}}{2 * k_{Layer\,2}} + \frac{1}{h_{surr}}} \tag{4}$$

where $t_{Layer\,2}$ is the thickness of Layer2, $k_{Layer\,2}$ is the thermal conductivity of Layer2 and h_{surr} is the convective loss from the stack to the air. The overall heat transfer coefficient for the heat coming from Layer1 is:

$$U_{Layer\,1} = \frac{1}{\frac{t_{Layer\,2}}{2 * k_{Layer\,2}} + \frac{t_{Layer\,1}}{2 * k_{Layer\,1}}} \tag{5}$$

The overall heat transfer coefficient for the heat coming from Layer3 is:

$$U_{Layer\,3} = \frac{1}{\frac{t_{Layer\,3}}{2 * k_{Layer\,3}} + \frac{t_{Layer\,2}}{2 * k_{Layer\,2}}} \tag{6}$$

If the layer conducts electricity (such as the contact layer), then there is an additional heat generation in Layer2 ($Q_{res\_Layer\,2}$) due to electrical resistance, which can be calculated as:

$$Q_{res\_Layer\,2} = (iA)^2 \frac{\rho_{res\_Layer\,2} t_{Layer\,2}}{A} \tag{7}$$

where i is the current density, A is the area of the layer, $\rho_{res\_Layer\,2}$ is the specific resistance of the material and $t_{Layer\,2}$ is the thickness of the layer. There is no heat generated in the end plate, contact or gasket layers. However, in some fuel cell stack designs, the end plate may be heated, therefore, an additional heat generation term would need to be added to the model formulation.

2.2.6. Mass Balances

Accurate mass balances are required to accurately predict species and heat transfer through the fuel cell stack. The mass balance equations (28 – 40) are used both for the outlet and inlet of each fuel cell stack layer, except for the GDL, catalyst and membrane layers where the diffusive mass flux is substituted into the appropriate equation in this section to get the rate of mass accumulation. The volumetric flow rate is first converted to a molar flow rate using the ideal gas law [10]:

$$n_{H2\_in} = \frac{PV}{RT} \tag{28}$$

For transient mass balances, the total molar accumulation can be written as:

$$\frac{dn_{tot}}{dt} = n_{tot\_in} - n_{tot\_out} \tag{29}$$

The rate of H_2 accumulation is:

$$\frac{d}{dt}(x_{H2}n_{tot}) = x_{H2\_in}n_{tot\_in} - x_{H2\_out}n_{tot\_out} \tag{30}$$

The rate of H_2O accumulation is:

$$\frac{d}{dt}(x_{H2O}n_{tot}) = x_{H2O\_in}n_{tot\_in} - x_{H2O\_out}n_{tot\_out} \tag{31}$$

The inlet and outlet molar flow rates can be calculated using the following equations:

Calculate the vapor pressure of the inlet water vapor:

$$P_{H2Ov\_in} = \phi_{in}P_{sat}(T_{H2O\_in}) \tag{32}$$

The mole fraction of the water vapor is:

$$X_{H2Ov\_in} = \frac{P_{H2Ov\_in}}{P_{tot}} \tag{33}$$

The mole fraction of the liquid water is:

$$X_{H2Ol\_in} = \frac{X_{H2Ov\_in} * P_{sat}(T_{H2O\_in})}{P_{tot}} \tag{34}$$

The total mole fraction of water is:

$$X_{H2O\_in} = X_{H2Ov\_in} + X_{H2Ol\_in} \tag{35}$$

The mole fraction of hydrogen is:

$$X_{H2\_in} = 1 - X_{H2O\_in} \tag{36}$$

The molar flow rate of hydrogen is:

$$n_{H2\_in} = x_{H2\_in}n_{tot\_in} \tag{37}$$

The total molar flow rate of water is:

$$n_{H2O\_in} = x_{H2O\_in}n_{tot\_in} \tag{38}$$

The molar flow rate of water vapor is:

$$n_{H2Ov\_in} = X_{H2Ov\_in} n_{H2O\_in} \tag{39}$$

The molar flow rate of liquid water is:

$$n_{H2Ol\_in} = X_{H2Ol\_in} n_{H2O\_in} \tag{40}$$

2.2.7. Heat transfer to gases

The outlet fluid temperature was calculated using the following:

$$Q_f = k_f * A * \left(T_{Layer} - T_{f,in}\right) \tag{41}$$

where Q_f is the heat flow from the plate, k_f is the conductivity of the gas or fluid, A is the area of the layer, T_{Layer} is the temperature of the layer and $T_{f,in}$ is the inlet gas or fluid temperature.

$$T_{f,out} = \frac{Q_f d \pi L}{4 n_{tot} c_{p,f}} + T_f \tag{42}$$

where d is the layer thickness, L is the length of the layer, and $c_{p,f}$ is the specific heat of the fluid.

2.2.6. Pressure Drop

In a typical flow channel, the gas moves from one end to the other at a certain mean velocity. The pressure difference between the inlet and outlet drives the fluid flow. By increasing the pressure drop between the outlet and inlet, the velocity is increased. The flow through bipolar plate channels is typically laminar, and proportional to the flow rate. The pressure drop can be approximated using the equations for incompressible flow in pipes:

$$\Delta P = f \frac{L_{chan}}{D_H} \rho \frac{\bar{v}^2}{2} + \sum K_L \rho \frac{\bar{v}^2}{2} \tag{10-4}$$

where f is the friction factor, Lchan is the channel length, m, D_H is the hydraulic diameter, m, ρ is the fluid density, kg/m3, $\bar{v}$ is the average velocity, m/s, and K_L is the local resistance.

The hydraulic diameter for a circular flow field can be defined by:

$$D_H = \frac{4 \times A_c}{P_{cs}} \tag{10-5}$$

where A_c is the cross-sectional area, and P_{cs} is the perimeter. In this work, the flow field channels are rectangular, and the inlet channels through the plates are circular. For rectangular channels, the hydraulic diameter can be defined as:

$$D_H = \frac{2 w_c d_c}{w_c + d_c} \tag{10-6}$$

where w_c is the channel width, and d_c is the depth.

The channel length can be defined as:

$$L_{chan} = \frac{A_{cell}}{N_{ch}(w_c + w_L)} \tag{10-7}$$

where A_{cell} is the cell active area, N_{ch} is the number of parallel channels, wc is the channel width, m, and w_L is the space between channels, m.

The friction factor can be defined by:

$$f = \frac{56}{\mathrm{Re}} \qquad (10\text{-}8)$$

Liquid or gas flow confined in channels can be laminar, turbulent, or transitional and is characterized by an important dimensionless number known as the Reynold's number (Re). This number is the ratio of the inertial forces to viscous forces and is given by:

$$\mathrm{Re} = \frac{\rho v_m D_{ch}}{\mu} = \frac{v_m D_{ch}}{\nu} \qquad (10\text{-}12)$$

where v_m is the characteristic velocity of the flow (m/s), Dch is the flow channel diameter or characteristic length (m), ρ is the fluid density (kg/m3), μ is the fluid viscosity [kg/(m*s or N* s/m2], and ν is the kinematic viscosity (m2/s). When Re is small (< 2000), the flow is laminar. When Re greater than 4000, the flow is turbulent, which means that it has random fluctuations. When Re is between 2000 and 4000, it is known to be in the "transitional" range, where the flow is mostly laminar, with occasional bursts of irregular behavior. It is found that regardless of channel size or flow velocity, f * Re = 16 for circular channels. The flow in fuel cell channels usually falls in the laminar flow regime.

The velocity (m/s) in a fuel cell channel near the entrance of the cell is:

$$v = \frac{v_{H2\_in}}{A_{ch}} \quad \text{where} \quad A_{ch} = \frac{1}{2}\pi r^2$$

where r is the radius of the channel.

2.2.6. Charge Transport

Most models neglect conductivity calculations, since most metallic and carbon-based fuel cell layers have good conductivity. However, a rigorous model should include this calculation since it can become a limiting factor due to geometry or composition. Ohm's law can be used to take this into account:

$$\frac{\partial \Phi_1}{\partial x} = -\frac{i}{\sigma_0} \qquad (9\text{-}46)$$

where ε_1 and σ_0 are the volume fraction and electrical conductivity, respectively. All electrochemically conductive layers in the fuel cell (besides the MEA layers) will use Equation.

2.2.2. Bipolar plate

The bipolar or flow field plates separate the reactant gases of adjacent cells, connect the cells electrically, and act as a support structure. The bipolar plates have reactant flow channels on both sides, forming the anode and cathode compartments of the unit cells on the opposing sides of the bipolar plate. Flow channel geometry affects the reactant flow velocities, mass transfer, and fuel cell performance. Bipolar plate materials must have high conductivity and be impermeable to gases. The material should also be corrosion-resistant and chemically inert due to the presence of reactant gases and catalyst. An illustration of the energy balance is shown in Fig. 5 [10]:

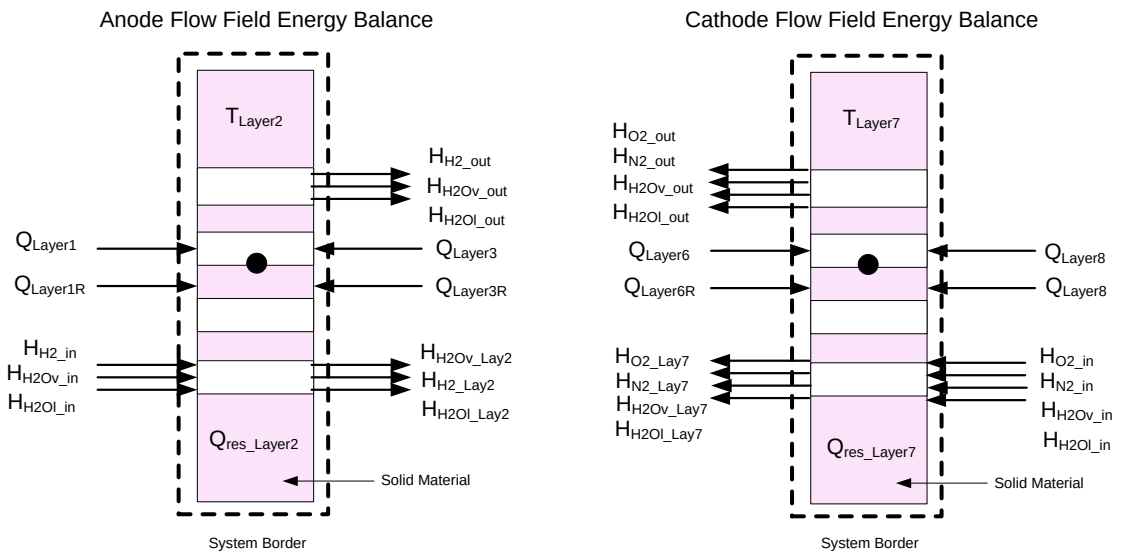

Fig. 5. Anode and Cathode flow field plate energy balance

The bipolar plate has both conductive and convective heat transfer due to the gas channels in the plate. The percentage of the bipolar plate that has channels affects the heat transfer of the overall plate, therefore, this is accounted for by calculating the effective cross-sectional area for conduction heat transfer, A_{1R}, which represent the area of the solid material in contact with the Layer1 and Layer3. The equation for heat transfer in the anode bipolar plate can be written as [10]:

$$(cp_{avg}(n_{gases}+n_{liq})+\rho_{Layer\,2}(A_{Layer\,2}t_{Layer\,2})cp_{Layer\,2})\frac{dT_{Layer\,2}}{dt}=Q_{Layer\,1}+Q_{Layer\,1R}+Q_{Layer\,3}+Q_{Layer\,3R}+Q_{res\_Layer\,2}+$$
$$H_{H2\_in}+H_{H2Ov\_in}+H_{H2Ol\_in}-H_{H2\_Lay3}-H_{H2Ov\_Lay3}-H_{H2Ol\_Lay3}-H_{H2\_out}-H_{H2Ov\_out}-H_{H2Ol\_out} \quad (8)$$

where $\rho_{Layer\,2}$ is the density of Layer2, A is the area of Layer2, $cp_{Layer\,2}$ is the specific heat capacity of Layer2, $Q_{Layer\,1}$ is the heat flow from Layer1 to the channels, $Q_{Layer\,1R}$ is the heat flow from Layer1 to the solid material, $Q_{Layer\,3}$ is the heat flow from Layer3 to

the channels, $Q_{Layer\,3R}$ is the heat flow from Layer3 to the solid material, $Q_{res\_Layer\,2}$ is the heat generation in the layer due to electrical resistance, and H_A is the enthalpy of component A coming into or out of the Layer2. The derivative on the left side is the rate of change of control volume temperature ($dT_{Layer\,2}/dt$). The heat flows coming from the right and left layer will transfer a different amount of heat from the layer to the solid and gas flow in the channels. The equation for heat transfer in the cathode bipolar plate can be written in a similar manner [10]:

$$(cp_{avg}(n_{gases}+n_{liq})+\rho_{Layer\,7}(A_{Layer\,7}t_{Layer\,7})cp_{Layer\,7})\frac{dT_{Layer\,7}}{dt}=Q_{Layer\,6}+Q_{Layer\,6R}+Q_{Layer\,8}+Q_{Layer\,8R}+Q_{res\_Layer\,7}+H_{O2\_in}+H_{N2\_in}+H_{H2Ov\_in}+H_{H2Ol\_in}-H_{O2\_2}-H_{N2\_2}-H_{H2Ov\_2}-H_{H2Ol\_2}-H_{O2\_out}-H_{N2\_out}-H_{H2Ov\_out}-H_{H2Ol\_out} \quad (8)$$

The heat flows are written in a similar manner for both the anode and cathode flow field plates. For the anode shown in Fig., The heat flow from Layer1 to the channels is:

$$Q_{Layer\,1}=U_{Layer\,1}A_{void}(T_{Layer\,1}-T_{Layer\,2}) \quad (9)$$

where A_{void} is the area of the channels. The heat flow from Layer1 to the solid material is:

$$Q_{Layer\,1R}=U_{Layer\,1R}A_{1R}(T_{Layer\,1}-T_{Layer\,2}) \quad (10)$$

where A_{1R} is the area of the solid. The heat flow from Layer3 (GDL) to the channels is:

$$Q_{Layer\,3}=U_{Layer\,3}A_{void}(T_{Layer\,3}-T_{Layer\,2}) \quad (11)$$

The heat flow from Layer3 (GDL) to the solid material is:

$$Q_{Layer\,3R} = U_{Layer\,3R} A_{1R} (T_{Layer\,3} - T_{Layer\,2}) \tag{12}$$

where A_{void} is the area of the channels in the plate, and A_{1R} is the area of the solid material. The heat generation in Layer2 ($Q_{res\_Layer\,2}$) due to electrical resistance is:

$$Q_{res\_Layer\,2} = (iA)^2 \frac{\rho_{res\_Layer\,2} t_{Layer\,2}}{A_{1R}} \tag{13}$$

where i is the current density, A is the area of the layer, $\rho_{res\_Layer\,2}$ is the specific resistance of the material and $t_{Layer\,2}$ is the thickness of the layer.

The enthalpy of each gas or liquid flow into or out of the layer can be defined as:

$$H_A = n_A h_A T_{Layer\,2} \tag{14}$$

where H_A is the enthalpy of the stream entering or leaving the layer, n_A is the molar flow rate of A, h_A is the enthalpy of A at the temperature of the layer (T_{Layer}).

The overall heat transfer coefficient terms can be calculated as:

$$U_{Layer\,1R} = \frac{1}{\frac{t_{Layer\,1}}{2 * k_{Layer\,1}} + \frac{t_{Layer\,2}}{2 * k_{Layer\,2}}} \tag{15}$$

$$U_{Layer\,1} = \frac{1}{\frac{t_{Layer\,1}}{2 * k_{Layer\,1}} + \frac{1}{h_l}} \tag{16}$$

$$U_{Layer\,3R} = \frac{1}{\frac{t_{Layer\,3}}{2 * k_{Layer\,3}} + \frac{t_{Layer\,2}}{2 * k_{Layer\,2}}} \tag{17}$$

$$U_{Layer\,3} = \frac{1}{\frac{t_{Layer\,3}}{2 * k_{Layer\,3}} + \frac{1}{h_l}} \tag{18}$$

The calculation of the thermal mass of the gas/liquid mixture is as follows:

$$thermal\_mass = cp_{avg}\,(n_{gases} + n_{liq}) \tag{19}$$

where cp_{avg} is the average specific heat of the gases (hydrogen and water) at the temperature of Layer2. The molar flow rate of the gases at the temperature of the Layer2 can be calculated by:

$$n_{gases} = \frac{PV_{gases}}{RT_{Layer\,2}} \tag{20}$$

where $V_{gases} = \varepsilon V_{void}$ is the volume of the gases in the channel, ε is the void fraction and V_{void} is the volume of the channel space, and is defined by:

$$V_{void} = A_{void}\, t_{Layer\,2} \tag{21}$$

The molar flow rate of the liquid in the channels in Layer2 is given by:

$$n_{liq} = \frac{V_{liq}\rho_{liq}}{MW_{H2O}} \tag{22}$$

where the volume of gases can be calculated by:

$$V_{liq} = V_{void} - V_{gases} \tag{23}$$

2.2.6. Mass Balances

The mass balance equations for the anode and cathode flow field plates are similar to Equations, except that there is an additional term for the mass flows going into the GDL

layers. The outlet flow are the gases leaving the stack. The mass flow is illustrated in Figure 6.

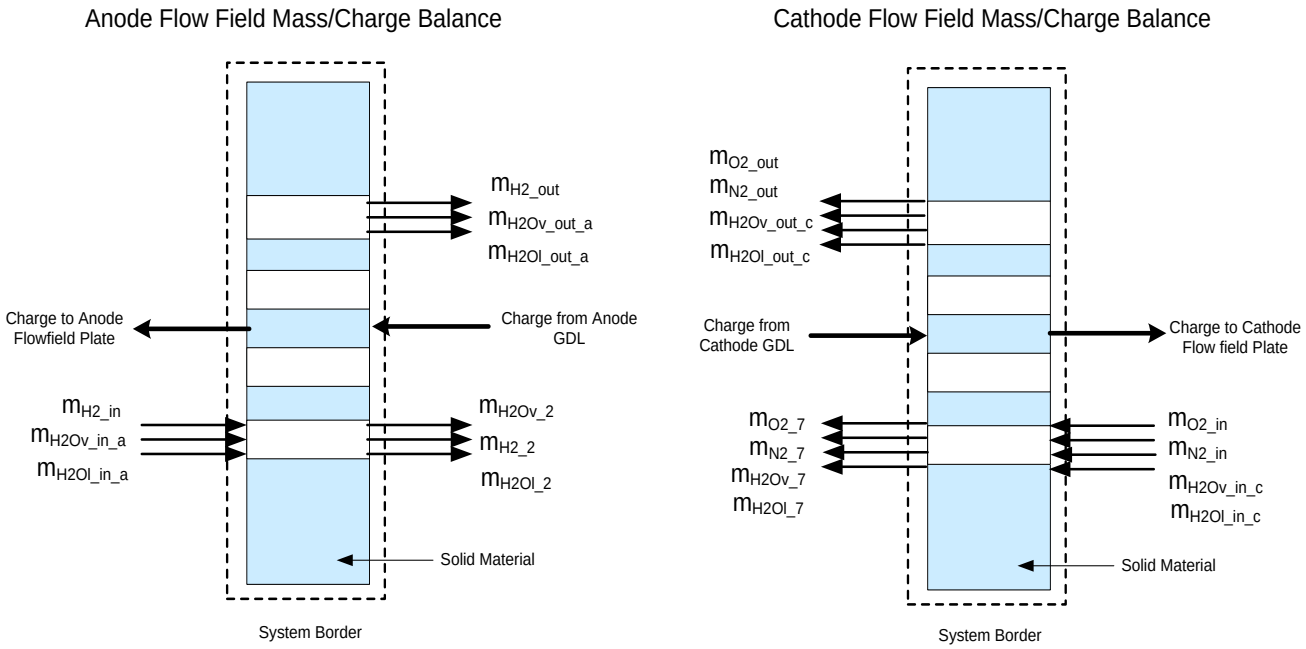

Figure 6. Cathode Flow field Plate Mass/Charge Balance

For the anode side:

For transient mass balances, the total molar accumulation can be written as:

$$\frac{dn_{tot}}{dt} = n_{tot\_in} - n_{tot\_out} - n_{tot\_2} \tag{29}$$

The rate of H_2 accumulation is:

$$\frac{d}{dt}(x_{H2}n_{tot}) = x_{H2\_in}n_{tot\_in} - x_{H2\_out}n_{tot\_out} - x_{H2\_2}n_{tot\_2} \tag{30}$$

The rate of H_2O accumulation is:

$$\frac{d}{dt}(x_{H2O}n_{tot}) = x_{H2O\_in}n_{tot\_in} - x_{H2O\_out}n_{tot\_out} - x_{H2O\_2}n_{tot\_2} \tag{31}$$

For the cathode side:

Rate of O_2 accumulation:

$$\frac{d}{dt}(x_{O2}n_{tot}) = x_{O2\_in}n_{tot\_in} - x_{O2\_out}n_{tot\_out} - x_{O2\_2}n_{tot\_2} \quad (31)$$

Rate of H_2O accumulation:

$$\frac{d}{dt}(x_{H2O}n_{tot}) = x_{H2O\_in}n_{tot\_in} - x_{H2O\_out}n_{tot\_out} - x_{H2O\_2}n_{tot\_2} \quad (31)$$

Rate of N_2 accumulation:

$$\frac{d}{dt}(x_{O2}n_{tot}) = x_{N2\_in}n_{tot\_in} - x_{N2\_out}n_{tot\_out} - x_{N2\_2}n_{tot\_2} \quad (31)$$

2.2.3. Anode/cathode diffusion media

The gas diffusion layer (GDL) is located between the flow field plate and the catalyst layer. This layer allows the gases and liquids to diffuse through it to reach the catalyst layer. The GDL has a much lower thermal conductivity than the bipolar plates and other metal components in the fuel cell, therefore, it partially insulates the heat-generating catalyst layers. When modeling the heat transfer through this layer, the solid portion has conductive heat transfer, and the gas/liquid flow has advective heat transfer. An illustration of the energy balance is shown in Fig. 7 [10, 11]:

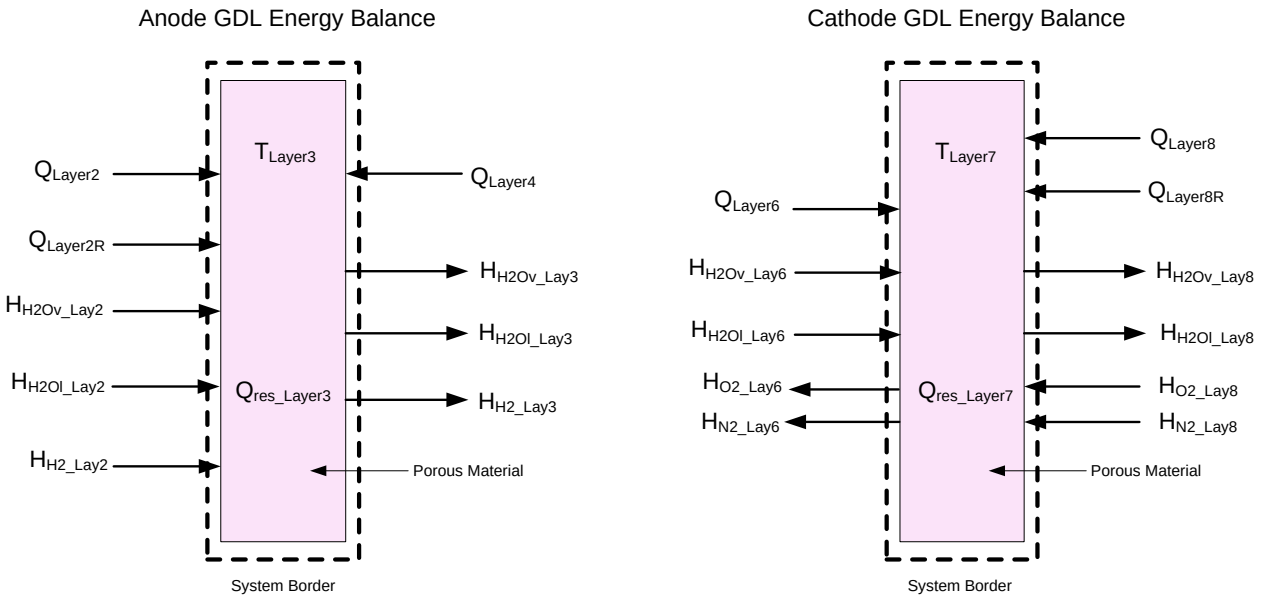

Fig. 7. GDL energy balance

Heat is generated in the GDL due to ohmic heating. Since the GDL has high ionic conductivity, ohmic losses are negligible compared with the catalyst and membrane layers. The overall energy balance equation for the anode can be written as:

$$(cp_{avg}(n_{gases}+n_{liq})+\rho_{Layer\,3}(A_{Layer\,3}t_{Layer\,3})cp_{Layer\,3})\frac{dT_{Layer\,3}}{dt}=Q_{Layer\,4}+Q_{Layer\,2}+Q_{Layer\,2R}+Q_{res\_Layer\,3}+H_{H\,2\_Lay\,2}+$$
$$H_{H2Ov\_Lay2}+H_{H2Ol\_Lay2}-H_{H\,2\_Lay3}-H_{H2Ov\_Lay3}-H_{H2Ol\_Lay3} \quad (24)$$

The overall energy balance equation for the cathode can be written as:

$$(cp_{avg}(n_{gases}+n_{liq})+\rho_{Layer\,3}(A_{Layer\,3}t_{Layer\,3})cp_{Layer\,3})\frac{dT_{Layer\,3}}{dt}=Q_{Layer\,3}+Q_{Layer\,3}+Q_{Layer\,1R}+Q_{res\_Layer\,3}+H_{O\,2\_2}+$$
$$+H_{N\,2\_2}+H_{H2Ov\_2}+H_{H2Ol\_2}-H_{O2\_3}-H_{N\,2\_3}-H_{H2Ov\_3}-H_{H2Ol\_3}$$

2.2.6. Mass Balances

The same mass balance equations are used for the anode and cathode GDL layer, except the mass flow rates are obtained from the gas concentrations calculated using. The overall mass balances are illustrated in Figure 8.

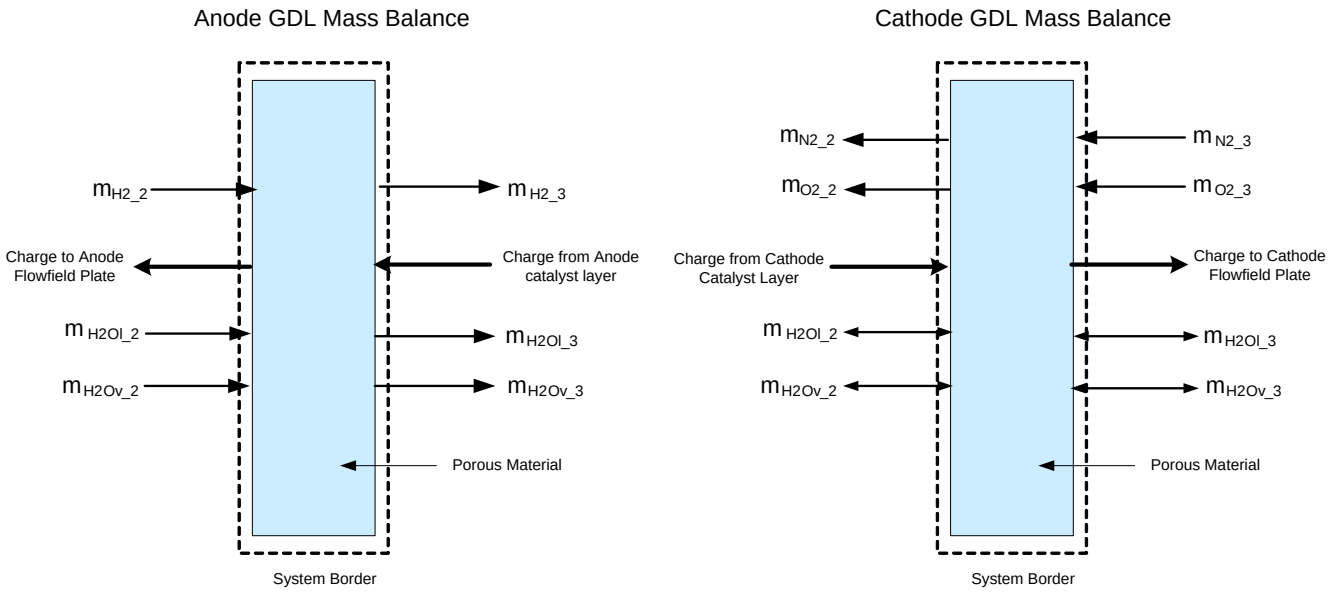

Figure 8. GDL Mass/Charge Balance

Knudsen diffusion and Stefan-Maxwell diffusion can be treated as mass-transport resistances in series, and are combined to yield:

$$\nabla x_i = -\frac{N_i}{c_T D_{K_i}^{eff}} + \sum_{j \neq i} \frac{x_i N_j - x_j N_i}{c_T D_{i,j}^{eff}} \tag{9-49}$$

where the $D_{K_i}^{eff}$ is the effective Knudsen diffusion coefficient. The porous media itself constitutes another species with zero velocity with which the diffusing species interact.

2.2.6. Charge Transport

Since the GDL layer is made of carbon, a charge transport relation is required. To account for porosity and tortuosity, the Bruggeman correction is used. Ohm's law is again used for charge transport:

$$\frac{\partial \Phi_1}{\partial x} = -\frac{i}{\varepsilon_1^{1.5}\sigma_0} \tag{9-46}$$

where ε_1 and σ_0 are the volume fraction and electrical conductivity, respectively. The Bruggeman correction is used in Equation 46 to account for porosity and tortuosity. Since the GDL is often coated with Teflon to promote hydrophobicity, carbon is the conducting phase and the Teflon is insulating.

2.2.4. Anode/cathode catalyst layer

The anode and cathode catalyst layer are a porous layer made of platinum and carbon. It is located on either side of the membrane layer. When modeling the heat transfer through this layer, the solid portion has conductive heat transfer, and the gas/liquid flow has advective heat transfer. Fig. 9 shows the energy balance of the catalyst layer [10].

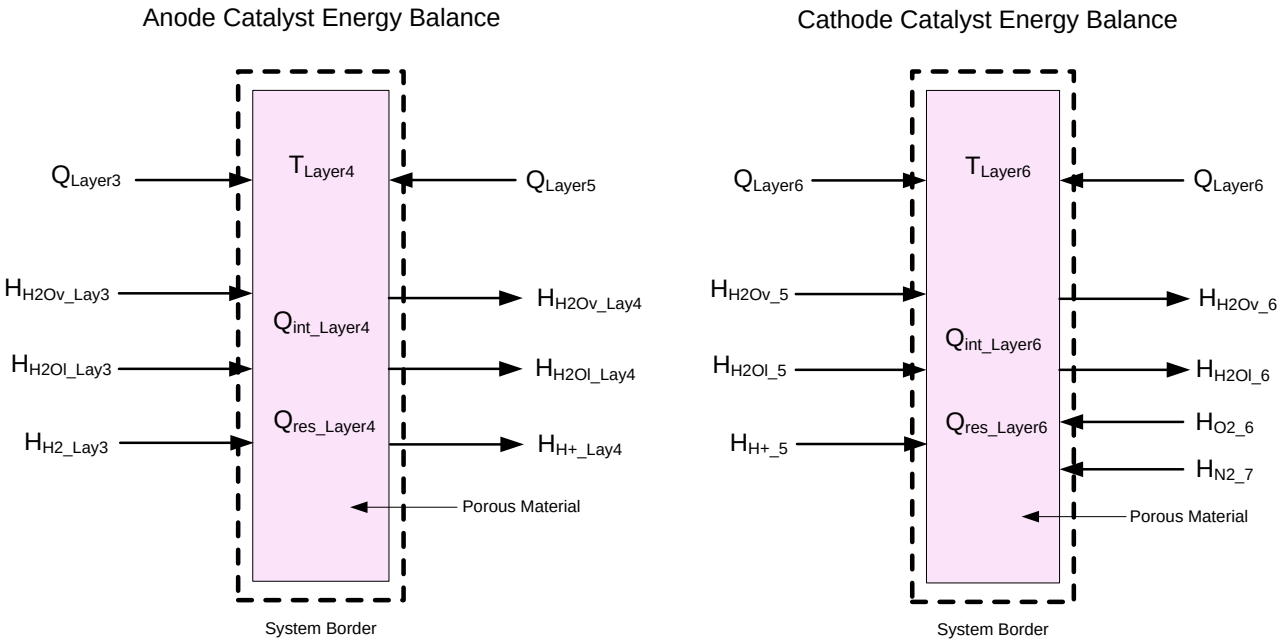

Fig. 9. Catalyst energy balance

The overall energy balance equation for the anode can be written as [10,11]:

$$(cp_{avg}(n_{gases}+n_{liq})+(\rho_{Layer\,3}A_{Layer\,3}t_{Layer\,3})cp_{Layer\,3})\frac{dT_{Layer\,3}}{dt}=Q_{Layer\,3}+Q_{mem}+Q_{\text{int}\_Layer\,3}+Q_{res\_Layer\,3}+$$
$$H_{H2\_3}+H_{H2Ov\_3}+H_{H2Ol\_3}-H_{H2\_4}-H_{H2Ov\_4}-H_{H2Ol\_4} \quad (25)$$

The overall energy balance equation for the cathode can be written as [10, 11]:

$$(cp_{avg}(n_{gases}+n_{liq})+(\rho_{a\_cat}A_{a\_cat}t_{a\_cat})cp_{a\_cat})\frac{dT_{a\_cat}}{dt}=Q_{a\_gdl}+Q_{mem}+Q_{a\_cat\_\text{int}}+Q_{res\_a\_cat}+$$
$$H_{O2\_3}+H_{N2\_3}+H_{H2Ov\_3}+H_{H2Ol\_3}-H_{O2\_4}-H_{N2\_4}-H_{H2Ov\_4}-H_{H2Ol\_4} \quad (25)$$

The heat generation in the catalyst layer is due to the electrochemical reaction and voltage overpotential. The heat generation term in the catalyst layer can be written as:

$$Q_{\text{int}\_Layer\,4}=\frac{i}{t_{Layer\,4}}\frac{T_{Layer\,4}\Delta S}{nF}+\eta \quad (26)$$

where $T_{Layer\,4}$ is the local catalyst temperature, i is the current density, $t_{Layer\,4}$ is the layer thickness, n is the number of electrons, F is Faraday's constant, ΔS is the change in entropy and η is the activation over-potential. The entropy change at standard state with platinum catalyst is taken as $\Delta S = 0.104$ J mol−1 K−1 for the anode, and $\Delta S = -326.36$ J mol−1 K−1 for the cathode. The activation over-potential (η) was calculated based on typical Tafel kinetics for a Pt-electrode.

2.2.6. Mass and Charge Transport

The mass and charge transport in the catalyst layer are interdependent, therefore, they are calculated together.

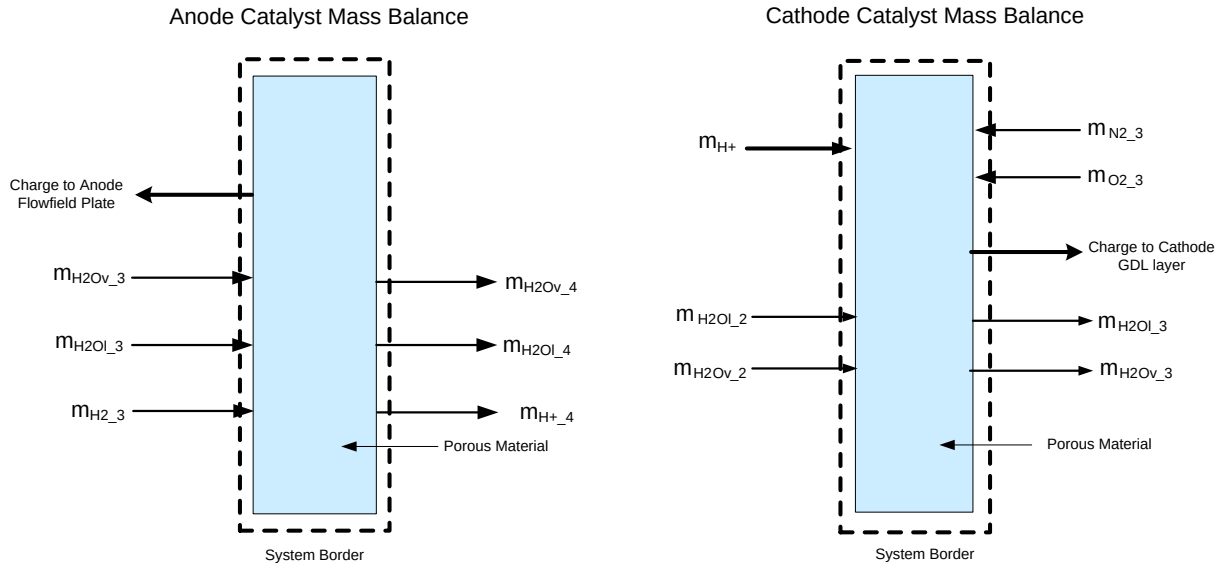

Figure 10. Cathode Catalyst Mass/Charge Balance

The voltage losses will now be calculated. The activation losses are estimated using the Butler-Volmer equation. For the anode:

$$\nabla \cdot i_2 = a_{1,2}(1-S)i_{anode}$$

$$i_{anode} = \left[\frac{p_{H2}}{p_{H2}^{ref}} \exp\left(\frac{\alpha_a F}{RT}\left(\Phi_1 - \Phi_2\right)\right) - \exp\left(\frac{-\alpha_c F}{RT}\left(\Phi_1 - \Phi_2\right)\right)\right]$$

For the cathode:

$$\nabla \cdot i_2 = a_{1,2}(1-S)i_{cathode}$$

$$i_{cathode} = \left[\frac{p_{O2}}{p_{O2}^{ref}} \exp\left(\frac{-\alpha_c F}{RT}\left(\Phi_1 - \Phi_2 - E_r\right)\right)\right]$$

As in the other layers, Ohm's law is used to calculate the potential:

$$\frac{\partial \Phi_1}{\partial x} = -\frac{i}{\varepsilon_1^{1.5}\sigma_0} \qquad (9\text{-}46)$$

where ε_1 and σ_0 are the volume fraction and electrical conductivity, respectively. The Bruggeman correction is used in Equation 46 to account for porosity and tortuosity.

The hydrogen oxidation reaction rate at the anode can be written as:

$$\nabla \cdot i_2 = a_{1,2} i_{h,1-2} E$$

$$\nabla \cdot N_{H_2,G} = -\frac{1}{2F} a_{1,2}(1-S)i_{anode} E$$

$$i_{anode} = \left[\frac{p_{H2}}{p_{H2}^{ref}} \exp\left(\frac{\alpha_a F}{RT}\left(\Phi_1 - \Phi_2\right)\right) - \exp\left(\frac{-\alpha_c F}{RT}\left(\Phi_1 - \Phi_2\right)\right)\right]$$

The liquid water cathode catalyst reaction can be written as:

$$\nabla \cdot N_{H2O,L} = -\frac{1}{4F} a_{1,2}(1-S)i_{cathode} E$$

$$i_{cathode} = \left[\frac{p_{O2}}{p_{O2}^{ref}} \exp\left(\frac{-\alpha_c F}{RT} \left(\Phi_1 - \Phi_2 - E_r \right) \right) \right]$$

Agglomerate models only consider effects that occur on the agglomerate scale. They assume a uniform reaction rate distribution. These models more accurately represent the structure of the catalyst layers than the simple porous electrode models. These are similar to the microscopic models, except the geometric arrangement is averaged and each phase exists in each control volume. The characteristic length scale of the agglomerate is assumed to be the same size and shape. In the model, the reactant or product diffuses through the electrolyte film surrounding the particle and agglomerate where it diffuses and reacts.

The equation for the porous catalysts has been used in the literature and is known to match experimental results. The porous catalyst equations can be used for both the anode and cathode, but this section reviews the equations for the cathode reaction. Equation 8-2 has been modified by the addition of an effectiveness factor, which allows for the actual rate of reaction to be written as:

$$\nabla \cdot i_2 = a_{1,2} i_{h,1-2} E \qquad (8\text{-}20)$$

Since the cathode reaction is a first-order reaction following Tafel kinetics, the solution of the mass conservation equation in spherical agglomerate yields an analytical expression for the effectiveness factor:

$$E = \frac{1}{3\phi^2} (3\phi \coth(3\phi) - 1) \qquad (8\text{-}21)$$

where ϕ is the Thiele modulus for the system, and can be expressed as:

$$\phi = \zeta \sqrt{\frac{k'}{D_{O2,agg}^{eff}}} \tag{8-22}$$

where ζ is the characteristic length of the agglomerate (volume per surface area), Ragg/3 for spheres, Ragg/2 for cylinders, and δagg for slabs, and k′ is a rate constant given by:

$$k' = \frac{a_{1,2} i_{0,Orr}}{4F c_{O2}^{ref}} \exp\left(-\frac{\alpha_c F}{RT} (\eta_{ORR,1-2}) \right) \tag{8-23}$$

where the reference concentration is that concentration in the agglomerate that is in equilibrium with the reference pressure:

$$c_{O2}^{ref} = p_{O2}^{ref} H_{O2,agg} \tag{8-24}$$

where HO2,agg is Henry's constant for oxygen in the agglomerate. If external mass transfer limitations can be neglected, then the surface concentration can be set equal to the bulk concentration, which is assumed uniform throughout the catalyst layer in simple agglomerate models.

2.2.6. Polarization curve

The first step is to calculate the Nernst voltage and voltage losses. To calculate the Nernst voltage for this example, the partial pressures of water, hydrogen and oxygen will be used. First calculate the saturation pressure of water:

$$\log P_{H_2O} = -2.1794 + 0.02953 * T_c - 9.1837 \times 10^{-5} * T_c^2 + 1.4454 \times 10^{-7} * T_c^3$$

Calculate the partial pressure of hydrogen:

$$p_{H_2} = 0.5 * (P_{H_2} / \exp(1.653 * i / (T_K^{1.334}))) - P_{H_2O}$$

Calculate the partial pressure of oxygen:

$$p_{O_2} = (P_{air} / \exp(4.192 * i / (T_K^{1.334}))) - P_{H_2O}$$

The ohmic losses (see Chapter 4) are estimated using Ohm's law:

$$V_{ohmic} = -(i * r)$$

The mass transport (or concentration losses -- see Chapter 5) can be calculated using the following equation:

$$V_{conc} = alpha1 * i^k * \ln\left(1 - \frac{i}{i_L}\right)$$

To insure that there are no negative values calculated for V_{conc} for the MATLAB program, the mass transport losses will only be calculated if $1 - \left(\frac{i}{i_L}\right) > 0$, else $V_{conc} = 0$.

The Nernst voltage can be calculated using the following equation:

$$E_{Nernst} = -\frac{G_{f,liq}}{2 * F} - \frac{R * T_k}{2 * F} * \ln\left(\frac{P_{H_2O}}{p_{H_2} * p_{O_2}^{1/2}}\right)$$

Since all of the voltage losses had a (-) in front of each equation, the actual voltage is the addition of the Nernst voltage plus the voltage losses:

$$V = E_{Nernst} + V_{act} + V_{ohmic} + V_{conc}$$

2.2.5. Membrane Layer

The PEM fuel cell membrane layer is a persulfonic acid layer that conducts protons and separates the anode and cathode compartments of a fuel cell. The most commonly used type is DuPont's Nafion® membranes. The dominant mode of heat transfer in the membrane is conduction. An illustration of the energy balance is shown in Fig. 11 [10, 11]:

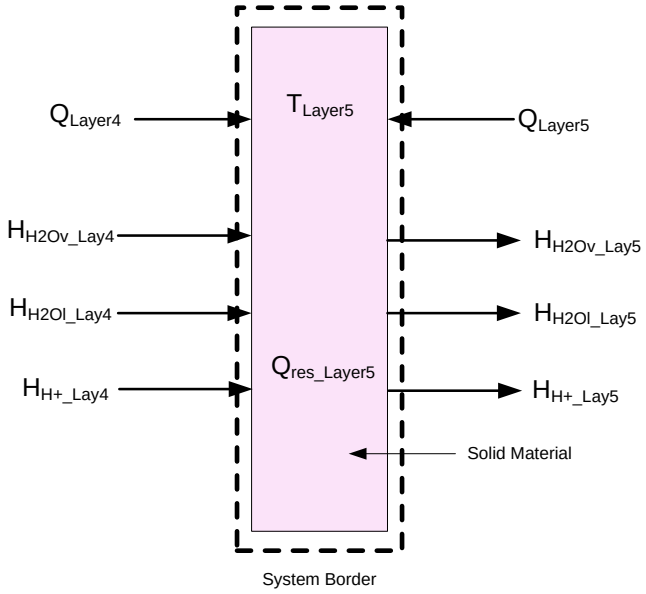

Fig. 11. Membrane energy balance

The overall energy balance equation can be written as:

$$(cp_{avg}(n_{gases}+n_{liq})+(\rho_{mem}A_{mem}t_{mem})cp_{mem})\frac{dT_{mem}}{dt}=Q_{a\_cat}+Q_{c\_cat}+Q_{res\_mem}+H_{H+\_4}+H_{H2Ov\_4}+H_{H2Ol\_4}-H_{H2\_5}-H_{H2Ov\_5}-H_{H2Ol\_5} \quad (27)$$

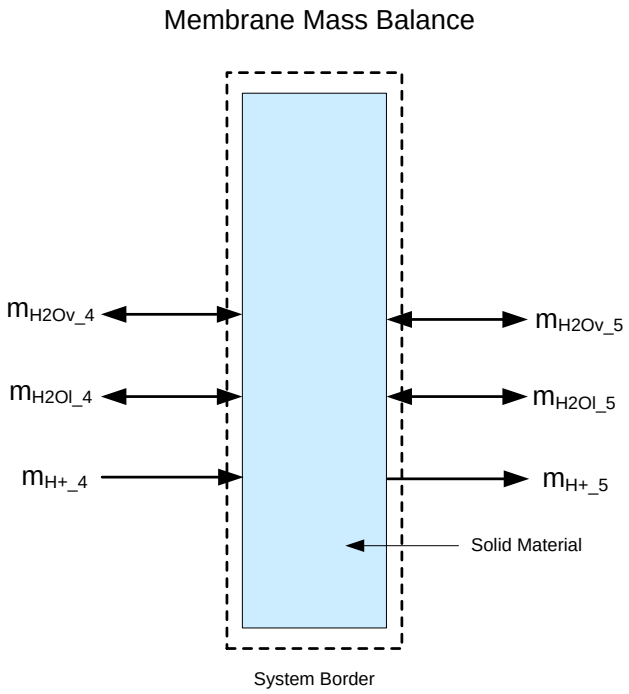

Figure 12. Membrane Mass/Charge Balance

The variables in this mass balance equation can be solved in a similar manner to the energy balance equations in the previous sections.

2.2.6. Mass transport

In polymer electrolyte membrane fuel cells, the two important fluxes are the proton flux and the water flux. The membrane needs to stay hydrated to ionically conduct hydrogen protons; therefore, it is very important to calculate the water flux in the electrolyte. In the Nafion membrane, two types of water flux are present: back diffusion and electroosmotic drag. Both fluxes can be accounted for by the following equation:

$$J_{H2O}^{M} = -D_{cH2O,T}\frac{\partial c_{H2O}^{m}}{\partial x} + n_{drag}\frac{i_x}{F} \qquad (7\text{-}10)$$

where n_{drag} is the measured drag coefficient, ix is the protonic current in the x direction, F is Faradays constant, $\lambda_{H2O/SO3}$ is the water content (molH2O/molSO3-), ρ_{dry}^{m} is the dry membrane density (kg/m3), $D_{cH2O,T}$ is the diffusion coefficient and Mm is the membrane molecular mass (kg/mol). The resistance of the electrolyte can be estimated using the water content, which can be described by:

$$n_{drag} = 2.5\frac{\lambda_{H2O/SO3}}{22} \tag{7-11}$$

$$\lambda_{H2O/SO3} = \frac{c_{H2O}^{m}}{\frac{\rho_{dry}^{m}}{M^{m}} - bc_{H2O}^{m}} \tag{7-12}$$

where b is the membrane extension coefficient in the x direction, which is determined experimentally, and the value is typically used.

$D_{cH2O,T}$ is the diffusion coefficient which includes a correction for the temperature and for the water content it is expressed in a fixed coordinate system with the dry membrane by:

$$D_{cH2O,I} = D'\left[\exp 2416\left(\frac{1}{303} - \frac{1}{T}\right)\right]\lambda_{H2O/SO3}\frac{1}{a}\frac{1}{17.81 - 78.9a + 108a^{2}} \tag{7-13}$$

where a is the activity of water, and D′ (m2/s) is the diffusion coefficient measured at constant temperature and in coordinates moving with the swelling of the membrane. D has been added to the above equation to ensure that water contents below 1.23 do not result in negative diffusion coefficients. D′ at 30 °C is written as:

$$D = 2.642276e(-13)\lambda_{H2O/SO3} \quad \text{for } \lambda_{H2O/SO3} \le 1.23 \tag{7-14}$$

$$D = 7.75e(-11)\lambda_{H2O/SO3} - 9.5e(-11) \quad \text{for } 1.23 < \lambda_{H2O/SO3} \le 6 \tag{7-15}$$

$$D = 2.5625e(-11)\lambda_{H2O/SO3} + 2.1625e(-10) \quad \text{for } 6 < \lambda_{H2O/SO3} \le 14 \tag{7-16}$$

The relation for the water activity within the membrane is given by the reciprocal of the sorption curve. As with the water vapor activity at the interfaces, the results from Springer et al. [8] for water vapor activity in Nafion 117 at 30 °C is given by:

$$a = \frac{1}{2160}c_1 + c_2\lambda_{H2O/SO3} + 216(c_3 - c_4\lambda_{H2O/SO3} + c_5{\lambda_{H2O/SO3}}^2)^{1/2})^{1/3} - 134183/2160/(c_1 + c_2\lambda_{H2O/SO3} + (216(c_3 - c_4\lambda_{H2O/SO3} + c_5{\lambda_{H2O/SO3}}^2)^{1/2})^{1/3} + \frac{797}{2160} \quad \text{for } \lambda_{H2O/SO3} \le 14$$

where c1 = -41956e4, c2 = 139968e3, c3=382482e6, c4=251739e3, c5=419904e6

$$a = 0.7143\lambda_{H2O/SO3} - 9.0021 \quad \text{for } 14 \le \lambda_{H2O/SO3} \le 16.8$$

$$a = 3 \quad \text{for } 16.8 \le \lambda_{H2O/SO3}$$

Thus, as soon as a current exists, the membrane is charged; and the concentration of protons remains constant. The charge of the protons equals that of the fixed charges. The diffusive molar flux for the protons (J_{H+}) can, therefore, be written as:

$$J_{H+} = -\frac{F}{RT}D_{H+}c_{H+}\frac{\partial\Phi_m}{\partial x} \tag{7-20}$$

Where Φ_m is the membrane proton potential and D_H is the proton diffusivity.

2.2.6. Charge transport

The equation for the proton potential is derived from Ohm's law. Both terms represent the proton flux divided by the membrane conductivity. The electroneutrality assumption allows the total molar proton flux to be related directly to current density and results in the first term. The second term containing u_m represents the convective flux of protons. Combined they result in the following equation:

$$\frac{\partial \Phi_m}{\partial x} = -\frac{i}{\sigma_m} + \frac{F}{\sigma_m} c_{H+} u^m$$

For the mixture (water and protons), the assumption is made that the momentum equation takes the form of the generalized Darcy relation:

where the Molar velocity of the mixture is:

$$u^m = -\frac{K k_r^g}{\mu}\left[\frac{\partial p}{\partial x} - \rho g \cos\theta\right]$$

where um is the mixture velocity, K is the absolute permeability of the porous medium, k_r^g is the relative permeability, g is the gravity, and θ is the angle that the x-axis (the direction of flow) makes to the direction of gravity. The mixture density and the dynamic viscosity of the mixture are written as:

Density for the mixture:

$$\rho = M_{H+} c_{H+} + M_{H2O} c_{H2O} \qquad (7\text{-}23)$$

Dynamic viscosity of the mixture:

$$\mu = \frac{M_{H+}c_{H+}}{\rho}\mu_{H+} + \frac{M_{H2O}c_{H2O}}{\rho}\mu_{H2O} \quad (7\text{-}24)$$

σ_m is the conductivity of the membrane and is written as a function of the temperature and the water content is: with σ_{m303}, the conductivity of the membrane at 303 K given by:

Electrical conductivity:

$$\sigma_m = \exp\left[1268\left(\frac{1}{303} - \frac{1}{T}\right)\right]\left[0.5139\lambda_{\frac{H_2O}{SO_3}} - 0.326\right], \text{ for } \lambda_{\frac{H_2O}{SO_3}} \geq 1$$

$$\sigma_m = \sigma_m\left[\lambda_{\frac{H_2O}{SO_3}} = 1\right], \text{ for } 0 < \lambda_{\frac{H_2O}{SO_3}} < 1$$

2.3. Numerical implementation

The mathematical equations for each layer were put into MATLAB. An array was created for the temperature, heat transfer coefficients, heat flows, enthalpies, mass flows, and pressures for each layer. Code was also incorporated to allow discretization of each of the layer into smaller control volumes or “slices”. Each layer or “slice” was assumed to abut the next one. The temperatures were assumed to be at the center of each “slice”, and the mass flow rates, pressure drop, velocity and charge transport at the boundaries of each control volume (see Figure 2). The set of equations were solved simultaneously using MATLAB’s ode45 ordinary differential equation solver. ode45 is based on an explicit Runge-Kutta (4,5) formula, the Dormand-Prince pair. It computes y(tn) in one step and needs only the solution at the immediately preceding time point, y(tn-1). The code allows

input of any number of control volumes or "slices" per layer. For the uniform distribution of nodes, the location of each node (x_i) is:

$$x_i = \frac{(i-1)}{(N-1)} L \quad \text{for } i = 1..N \tag{3-1}$$

where N is the number of nodes used for the simulation. The distance between adjacent nodes (Δx) is:

$$\Delta x = \frac{L}{N-1} \tag{3-2}$$

A control volume is defined around each node; the control surface bisects the distance between the nodes, as shown in Figure 2.

3.0 Stack parameters and verification

A numerical code was developed to investigate the effect of various stack materials and operating parameters on fuel cell heat transfer behavior. The code was validated by taking the I-V curve and layer temperature of a single cell fuel cell stack with a heated anode end plate. The stack dimensions and other parameters used in the simulations are summarized in Tables 1-7. Table 1 summarizes all the overall parameters for the single cell fuel cell stack.

Table 1. Stack parameters for the base case simulation

No. Cells	1	N/A
Clamping force	150	N-m
Nominal power	0.5	W
Voltage per cell	0.7	V/cell
Current density	600	mA/cm^2

Operating temperature	20	ºC
Operating pressure	1	atm

The properties of the surroundings used in the mode are summarized in Table 2.

Table 2. Parameters of surroundings

Variable	Description	Value	Units
Outside Temperature	Temperature of fuel cell stack surroundings.	298	K
Outside pressure	Pressure of fuel cell stack surroundings.	101,325.01	Pa
Heat coefficient	Convective loss from the stack to surroundings	17	W/m2-K

Properties of the hydrogen, oxygen and water were used in every layer in the fuel cell stack model. These properties are summarized in Table 3.

Table 3. Parameters of Hydrogen, Oxygen and Water

Variable	Hydrogen	Air	Water
Temperature of gas or liquid going into stack (K)	298	298	298
Humidity of gas or liquid going into stack	0.5	0.5	N/A
Pressure of gas going into stack (Pa)	101,325.01	101,325.01	N/A
Volumetric flow rate of gas or liquid going into stack (m^3/s)	1.7e-8	1e-8	N/A
Molecular weight (kg/mol)	1e-3		(8e-3
Viscosity (Pa-s)	8.6e-6 (98.8e-7 kg/ms)	8.6e-6	(8.91e-4 kg/ms)
Density (kg/m3)	972	1.3	
Thermal Conductivity (W/m-K)	0.165	0.223	
Specific heat capacity (J/kg-K)	300	1005	4190

The material parameters of the fuel cell stack layers are described in Table 4.

Table 4. Parameters of Fuel Cell Stack Layers

Fuel Cell Layer	Material	Thickness (m)	Area (m2)	Area of void (m2)	Density (kg/m^2)	Thermal Conductivity (W/m-K)	Specific heat capacity (J/kg-K)	Specific Resistance (ohm-m)
End plate	Polycarbonate	0.01	0.0064	0	1300	0.2	1200	0
Gasket	Black Conductive Rubber	0.001	0.001704	0	1400	1.26	1000	0
Flow field plate	SS	0.0005	0.003385	0.0016925	8000	16	500	7.2e-7
Diffusion media	Carbon Cloth	0.0004	0.0016	0.00128	2000	65	840	0.000014
Catalyst	Pt/C	0.000065	0.0016	0.00112	387	0.2	770	0.000014
Membrane	Nafion	0.00005	0.0016	0	1740	0.21	1100	0.1

Fuel Cell Layer	Material	Thickness (m)	Area (m2)	Area of void (m2)	Density (kg/m^2)	Thermal Conductivity (W/m-K)	Specific heat capacity (J/kg-K)	Specific Resistance (ohm-m)
Catalyst	Pt/C	0.000065	0.0016	0.00112	387	0.2	770	0.000014
Diffusion media	Carbon Cloth	0.0004	0.0016	0.00128	2000	65	840	0.000014
Flow field plate	SS	0.0005	0.003385	0.0016925	8000	16	500	7.2e-7
Gasket	Black Conductive Rubber	0.001	0.001704	0	1400	1.26	1000	0
End plate	Polycarbonate	0.01	0.0064	0	1300	0.2	1200	0

The flow field parameters were used in the mass transfer and pressure drop portions of the model and are listed in Table 5.

Table 5. Parameters Used for Flow field plates

Variable	Description	Value	Units
Reactant Flow Channel Dimensions			
Total Length	Total Channel length	24.63 (avg)	m
"L" bends in channel	No. "L" bends in channel	12/20/10	N/A
"U" bends in channel	No. "U" bends in channel	4/5	N/A
Length of straight sections	Length of straight channel sections	20.89	m
Cross-sectional area	Channel cross-sectional area	3.2258e-7	m^2
Perimeter	Channel Perimeter	0.0000419354	m

The membrane and proton properties used for the membrane portion of the model are shown in Table 6.

Table 6. Parameters Used for Membrane Layer

Variable	Description	Value	Units
Outside Temperature	Temperature of fuel cell stack surroundings.	298	K
Outside pressure	Pressure of fuel cell stack surroundings.	101,325.01	Pa
Proton Properties:			
Initial proton concentration	Initial proton concentration	1.2e-3	mol/m^3
Proton diffusivity	Proton diffusion coefficient	4.5e-5	cm^2/s
Membrane Properties:			
Density of membrane	Density of membrane	2,000	kg/m^3
Molecular weight of membrane	Molecular weight of membrane	1.1	Kg/mol SO_3

Variable	Description	Value	Units
Specific heat of membrane	Specific heat of membrane	852.63	J/kgK
Permeability	Permeability of membrane	1.8e-18	m^2
Initial saturation ratio	Initial saturation ratio	0.02	N/A

The parameters used for the catalyst agglomerate model and polarization curve are shown in Table 7.

Table 7. Parameters Used for the Catalyst Layer

Variable	Description	Value	Units
Agglomerate Properties:			
O2 Permeation	Oxygen permeation in agglomerate	1.5e-11	
H2 Permeation	Hydrogen permeation in agglomerate	2e-11	
Anode radius	Agglomerate radius in the anode	110e-5	
Cathode radius	Agglomerate radius in the cathode	110e-5	
Saturation	Saturation	0.6e-12	N/A
Anode transfer coefficient	Anode transfer coefficient	1	
Cathode transfer coefficient	Cathode transfer coefficient	0.9	
Gibbs function	Gibbs function in liquid form	-228,170	J/mol
Interfacial area	Electrode specific interfacial area	10,000	1/cm
Anode entropy change	Anode entropy change	0.104	J/mol-K
Cathode entropy change	Cathode entropy change	-326.36	J/mol-K

4.0 Results and discussion

All the tests conducted with the model used the parameters presented in Tables 1-7. The only condition that varied for each test presented in this section is the initial fuel cell layer temperatures.

4.1.5. Membrane layer results

Since the membrane contributes significantly to the overall fuel cell polarization curve performance, some of the results of the membrane portion of the model are included in this section. The four main variables that were studied in the membrane layer are the water concentration, the potential, temperature and pressure. Figures shows the variance of these four parameters over the thickness of the membrane. In figure, the temperature and pressure increase slightly. The water concentration also increases, and the potential decreases.

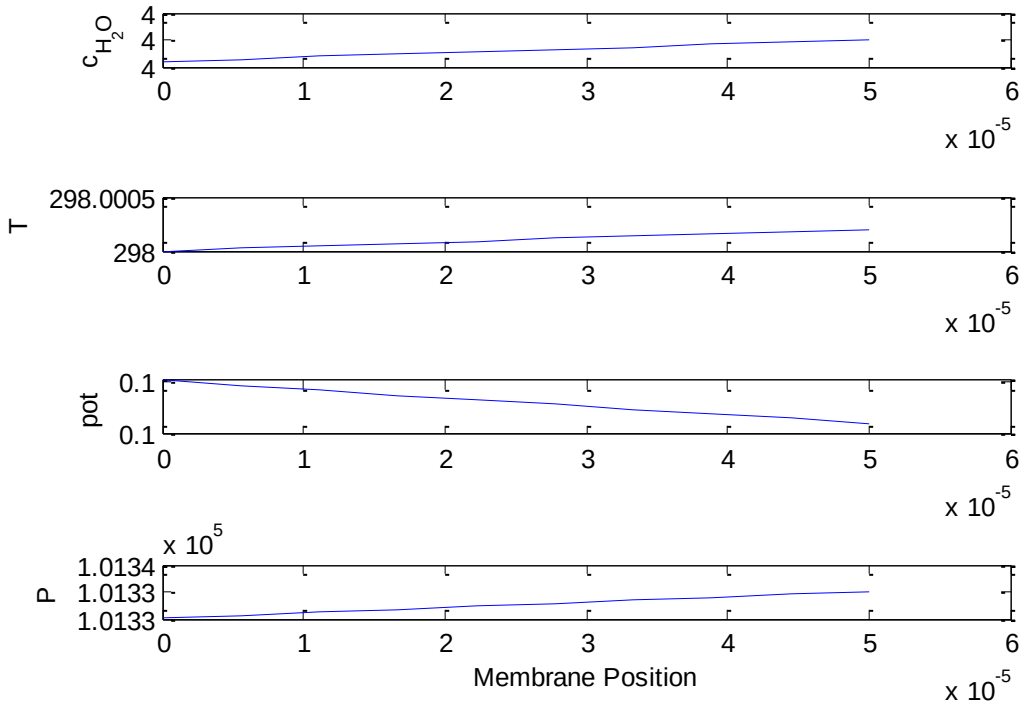

Figure 13. Water concentration, Temperature (298), potential and pressure (1 bar) across the membrane

Figure 13 shows the profiles of the variables at a higher temperature of 343 K. The water concentration increase is greater than in Figure 14.

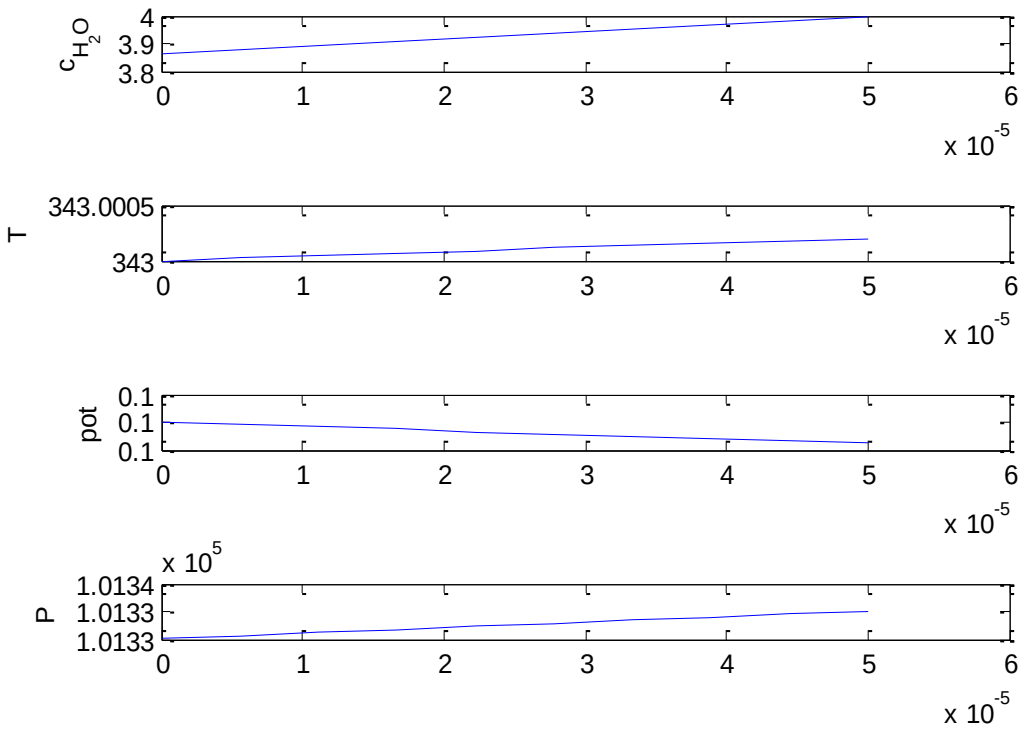

Figure 14. Water concentration, Temperature (343), potential and pressure (1 bar) across the membrane

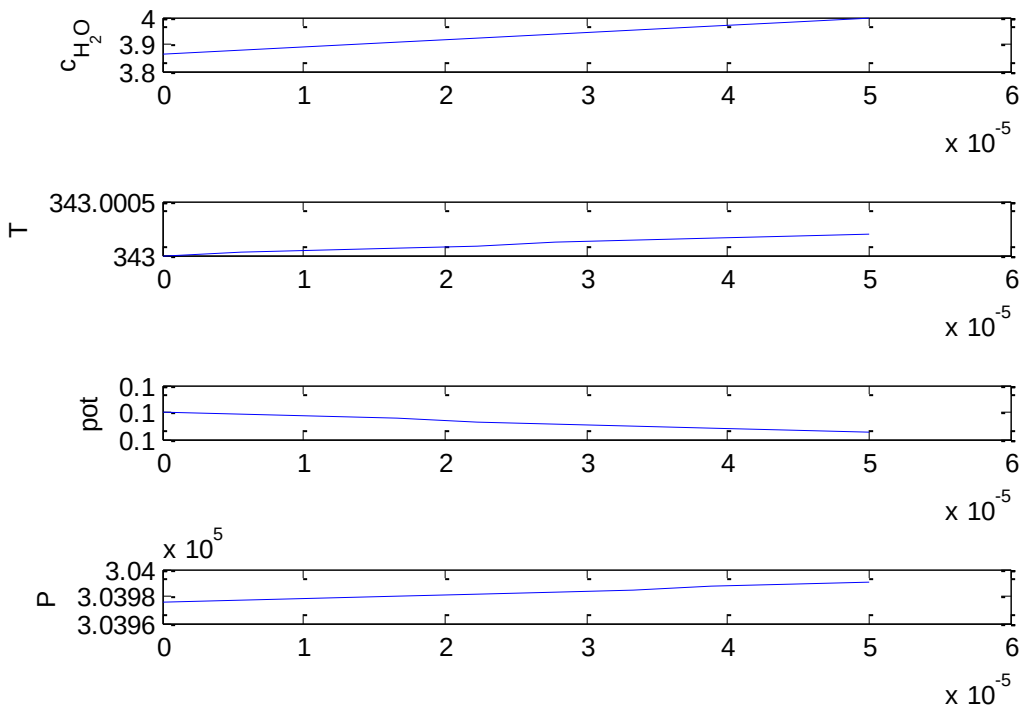

Figure 15. Water concentration, Temperature (343), potential and pressure (3 bar) across the membrane

4.1. Validation of the heat transfer numerical code

A single cell, air breathing fuel cell stack was assembled for fuel cell heat transfer and I-V tests. A five-layered MEA from Clean Fuel Cell Energy was used, which is composed of Nafion 112, GDL of carbon cloth material, and 1 mg/cm^2 of Pt loading on both anode and cathode. The active fuel cell area for the stack is 16 cm^2. The anode side end plate was heated using a custom-made aluminum heating block with two small cartridge heaters, controlled by an Omega CN616TC1 controller. An Omegaette HH311 RS-232 temperature and humidity meter with a type K thermocouple was placed onto the anode side of the MEA. The stack was then clamped together using clamping bolts with the

thermocouple left inside to monitor the MEA temperature. The Omegaette HH311 was also used to keep track of the room temperature and humidity. Measurements were taken of the aluminum heating block, and each end plate using a VWR infrared thermometer gun. Cell performance tests are conducted with 0.5 to 1.0 standard cubic centimeter per minute (SCCM) of hydrogen from an electrolyzer, with no additional humidification. All tests are taken at 25º C and ambient pressure. I–V curves of these cell performance tests with various anode end plate temperatures are plotted in Fig. 9. As expected, the electro-chemical performance increases as the fuel cell temperature increases.

4.1.1. Test 1

The aluminum heating block was placed against the anode end plate and heated to 35.2 ºC. The open circuit voltage measurement was taken, and then the temperatures of the MEA, and the end plates were recorded. The aluminum heating block was then removed, and the stack was allowed to cool for ten minutes. The temperatures were taken every minute continuously for 10 minutes. The temperature results of each end plate, and the MEA layers are shown in Fig 16. The temperature for the anode end plate seemed to linearly decrease during the ten minutes, the MEA layers steadily heated up, and the cathode end plate temperature fluctuated.

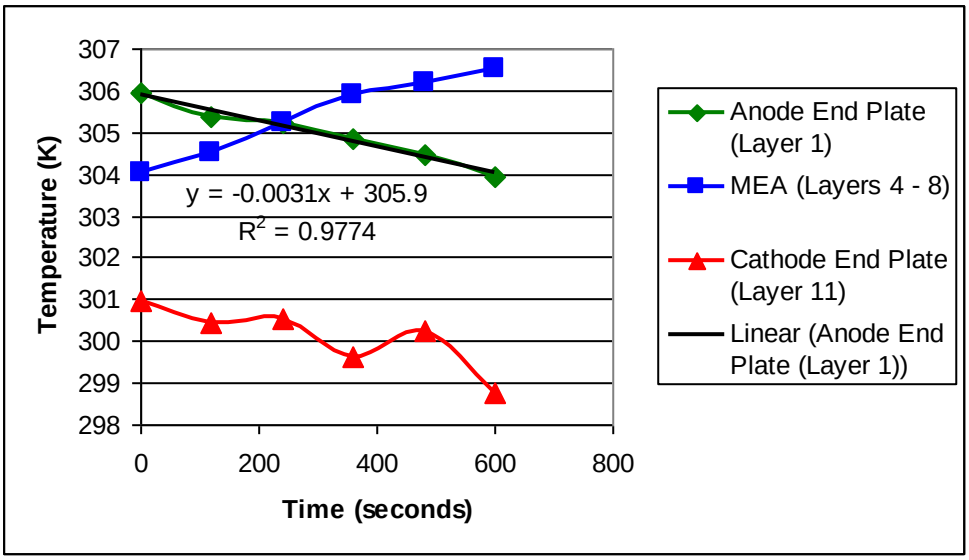

Fig. 16. Temperature distribution for Test 1

The parameters and material properties from Tables 1 and 2 were entered into the numerical model for the stack, and the temperature distribution was created. Since the anode end plate temperature input was unsteady over time, a trend line was fitted to the end plate temperature as shown in Fig 10. This equation was used in the model for the anode end plate temperature. The model was run for 360 and 600 seconds. The plots that were obtained are shown in Figs 17 and 18.

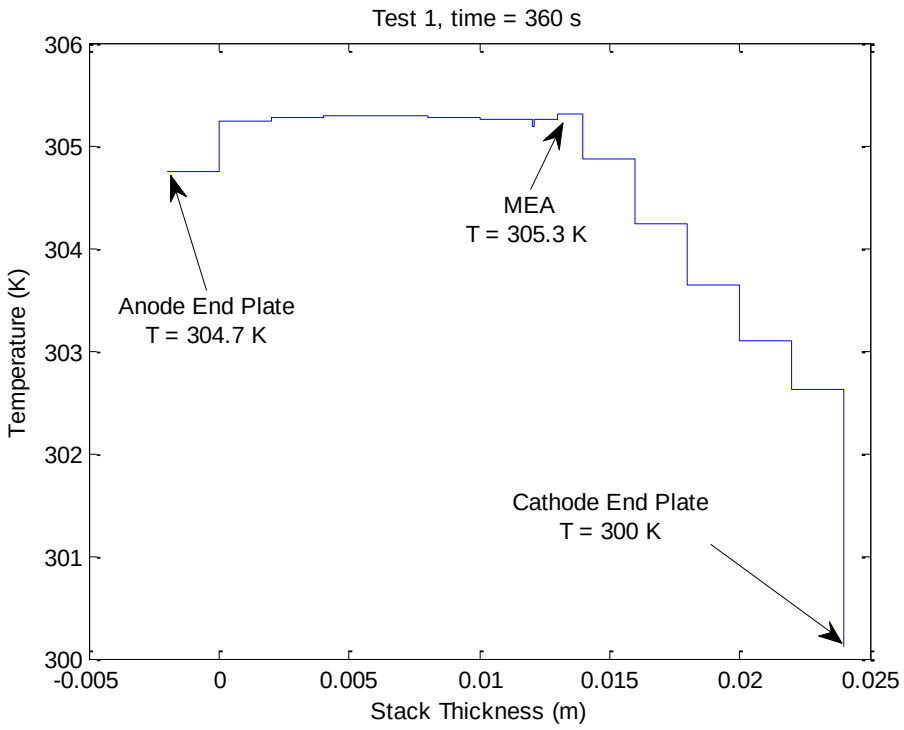

Fig. 17. Test 1 temperature distribution at 360 sec

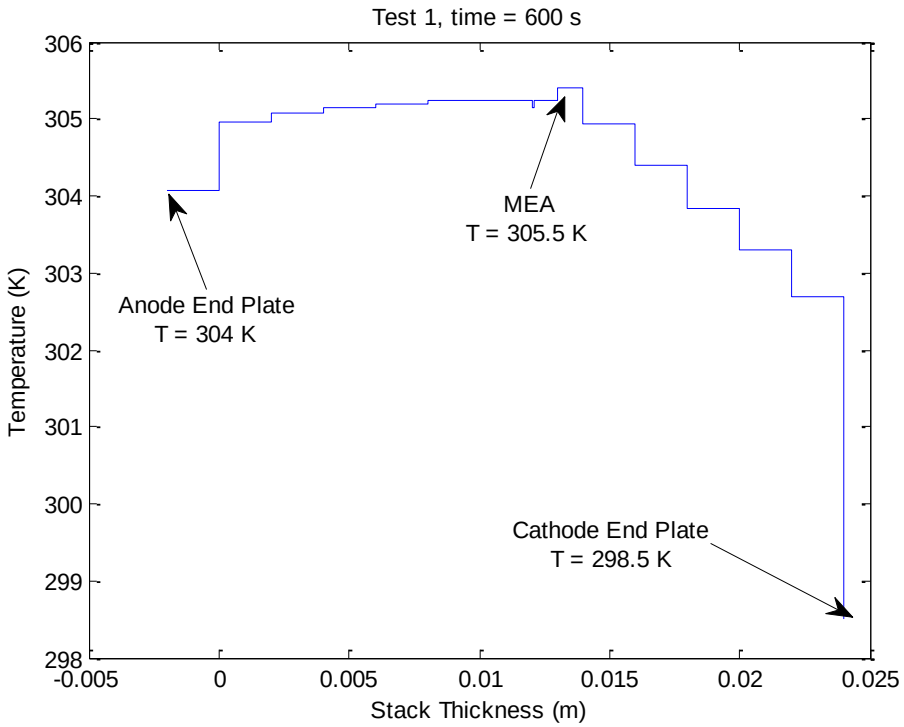

Fig. 18. Test 1 temperature distribution at 600 sec

Figure 19 shows a comparison of the average percent error for tests 1 – 4 for the anode and cathode end plates and the MEA layers. The anode end plate had the lowest average error with 0.63 % (range: 2.4% max, -0.43 % min). The average error for the MEA was the largest at 1.1 % (range: 3.0 % max, -0.19 % min). The average error for the anode end plate was 1.05 % (range: 3.4 % max, -3.2 % min). There was a significant min and max range for the cathode end plate due to a low and high value in the range, but the average percent error was still very good. The numerical model performed well with a minimal number of slices (5 – 12 for the end plates, 1 slice per MEA layer). Additional details about the heat transfer portion of the model was given in a previous paper.

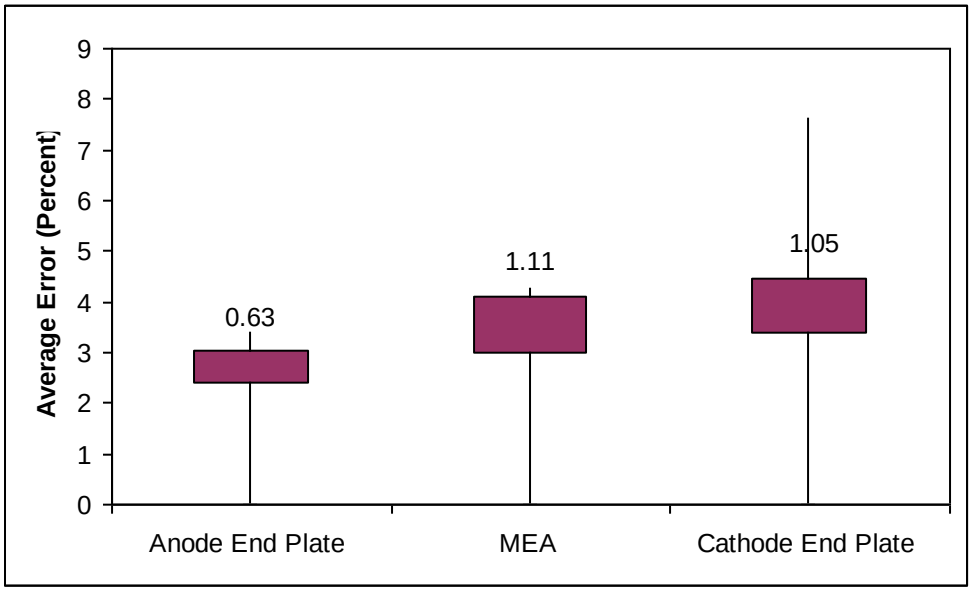

Fig 19. Average and range of error between model and experimental results (8 runs)

4.1. Validation of the overall electrochemical code

Figures 20 and 21 summarize the overall electrochemical code and show a good match between the model and experimental results.

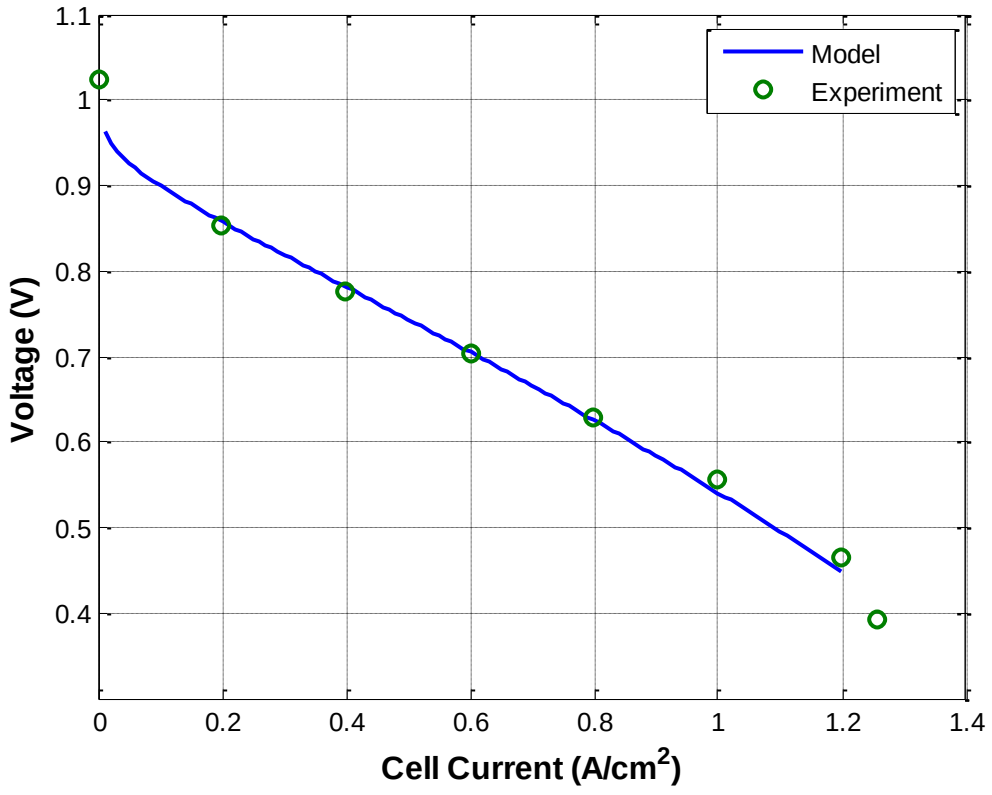

Fig 20. Stack #1: 16 cm2 stack at 298 C and 1 atm

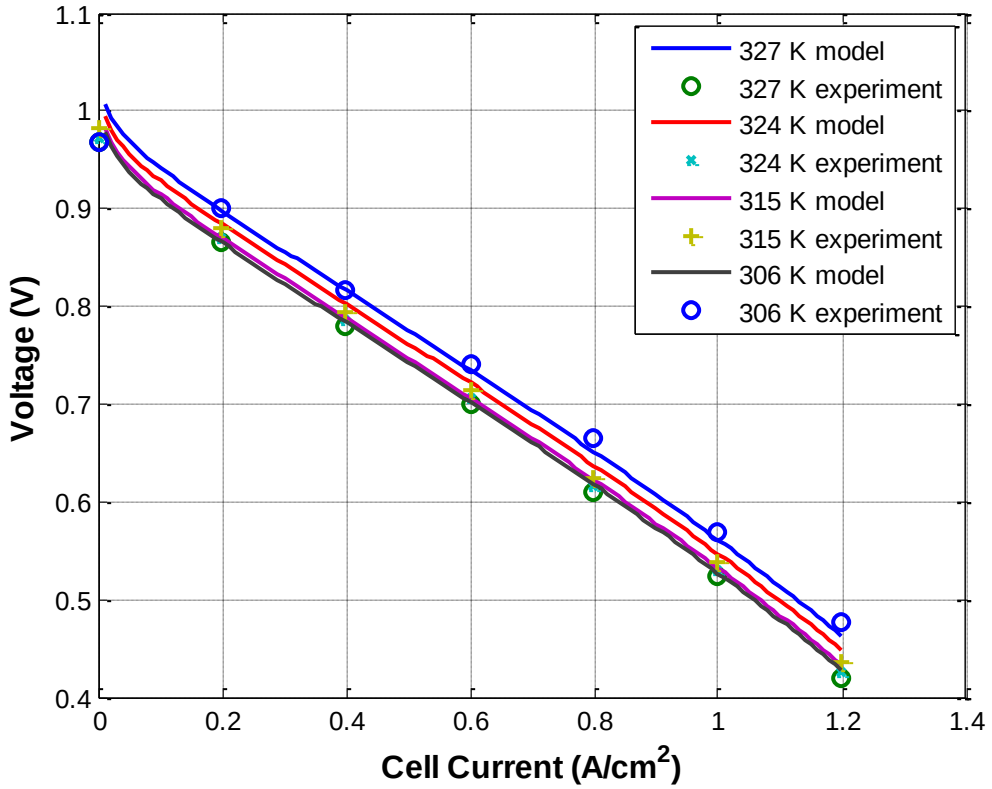

Fig 21. Stack #1: 16 cm^2 stack at 298 C and 1 atm

4.0 Conclusions

An overall fuel cell model for predicting electrochemical performance was created and validated using a 16 cm^2 fuel cell stack. A numerical model included energy, mass and charge balances for each fuel cell layer. To precisely model the electrochemical reactions, an agglomerate catalyst layer was included in the model using porous electrode equations. In addition, an empirical membrane model based upon water content was integrated into the model. The experimental validation consisted of experimentally examining the temperatures of the fuel cell layers and IV curves of the PEM fuel cell

stack. As the anode end plate temperature changed, the rest of the fuel cell stack layers and the electrochemical performance also changed. Results show that the numerical calculations agree well (< 1.5 % average) with the fuel cell stack heat and electrochemical tests. It is further shown that higher anode end plate temperatures result in layer temperature fluctuations through the fuel cell stack. Although the higher temperatures result in better electrochemical performance, the heat fluctuations within the stack make the fuel cell harder to control.

References

[1] G. Maggio, V. Recupero and C. Mantegazza, J. Power Sources 62 (1996), pp. 167–174.

[2] Y. Zhang, M. Minggao, Q. Lu, J. Luo and X. Li, App. Thermal Eng. 24 (2004), pp. 501–513.

[3] J. Park and X. Li, J. Power Sources 162 (2006), pp. 444–459.

[4] Y. Zong, B. Zhou and A. Sobiesiak, J. Power Sources 161 (2006), pp. 143–159.

[5] C. Graf, A. Vath and N. Nicoloso, J. Power Sources 155 (2006), pp. 52–59.

[6] M. Sundaresan and R.M. Moore, J. Power Sources 145 (2005), pp. 534–545.

[7] Y. Shan and S.Y. Choe, J. Power Sources 158 (2006), pp. 274–286.

[8] Y. Shan, S.Y. Choe and S.H. Choi, *J. Power Sources* **165** (2007), pp. 196–209.

[9] M. Khandelwal and M.M. Mench, J. Power Sources 161 (2006), pp. 1106–1115.

[10] C. S. Spiegel, PEM Fuel Cell Modeling and Simulation Using MATLAB (1st ed.), Elsevier Science (2008).

[11] F.P. Incropera and D.P. DeWitt, Fundamentals of Heat and Mass Transfer (4th ed.), John Wiley & Sons (1996).

[12] A.J. Bard and L.R. Faulkner, Electrochemical Methods: Fundamentals and Applications, John Wiley & Sons Inc., New York (1980).